Biomimetic and Biophysical Approach to Profile Metastatic Cancer Cell Migration

Thesis

Presented in Partial Fulfillment of the Requirements for Graduation with Honors Research Distinction at The Ohio State University

By

Jacob J. Enders

Undergraduate Program in Biomedical Engineering

The Ohio State University

2018

Thesis Committee

Jonathan Song, Advisor

Carlos Castro

Abstract

Cancer metastasis is a complex process by which cells in a primary tumor acquire an aggressive phenotype, and travel to distant, secondary sites in the body. One aspect of cancer metastasis is cell migration toward the vascular system, called invasion. Multiple modalities of single cell invasion exist, including amoeboid migration and mesenchymal migration. Amoeboid migration is less well understood, and in particular, the forces involved in amoeboid migration have yet to be fully elucidated at a subcellular scale. Cellular traction force microscopy, or CTFM, is one method used to probe migration forces. However, this approach is largely limited to two dimensions, and is limited by the size of the pillars on the substrate. To address these limitations, we developed a system using microfluidics and DNA origami capable of real-time force measurement of cell migration on a subcellular scale with a 10 pN resolution.

Microfluidic devices were made using soft lithography and replica molding in our laboratory. DNA origami were made using protocols developed by Michael Hudoba and Dr. Carlos Castro in the Nanoengineering and Biodesign Laboratory. The devices were imaged using TIRF microscopy to study dwell times of the sensors in the open and closed states, and the devices were analyzed with an AFM to determine that they are best suited for measuring shear forces. Further, the presence of streptavidin protein was found to have a significant effect on DOFS binding with a p-value less than 0.05. DOFS concentrations around 1 nM were found to provide the most coverage while minimizing structure

aggregation. Thus, our microfluidic devices are able to be functionalized with DNA origami force sensors with a high degree of attachment. This platform is thus capable of measuring cell migration and adhesion forces, and future work should harness this system to create 3D maps of cell migration to gain insight into invasion.

Dedication

To my uncle and childhood friend, William Moore.

Acknowledgments

I would like to thank my research mentor, Dr. Jonathan Song, for his years of guidance and support throughout my undergraduate education. In addition to research, I have learned so much from you, and for this I cannot thank you enough. I have truly enjoyed seeing our lab grow since I was a first-year student, and I look forward to reading about all the great work you accomplish in the future.

I would also like to thank my co-mentor, Dr. Carlos Castro and his former student, Dr. Michael Hudoba, for their assistance while working with the NanoDyn. Through my research, I have started to gain an understanding of the vast potential of DNA origami, and I look forward to seeing all that you accomplish with this technology. I would also like to thank Dr. Castro for serving as a member of the Eminence Faculty Network. This is a great program for Eminence Fellows, and we all greatly appreciate your mentorship.

To my parents, Susan Weber, William Enders, Gene Weber, and Marcy Enders, I am grateful for your many years of guidance. I am who I am because of all of you, someone who is driven to be successful and make a difference in the world.

This work was supported through funding from the Institute for Materials Research, the Second-Year Transformational Experience Program, and the College of Engineering Honors Research Committee at The Ohio State University.

Thank you all, it has truly been an honor.

Vita

Education

2014-18 B.S. Biomedical Engineering, *Summa Cum Laude*
The Ohio State University

Research and Work Experience

2017 Biomedical Engineering Summer Intern, Laboratory of Molecular Biophysics
National Institutes of Health, Biochemistry and Biophysics Center

2015-18 Student Researcher, Microsystems for Mechanobiology and Medicine Laboratory
The Ohio State University

2015-18 Undergraduate Teaching Assistant, Fundamentals of Engineering for Honors Program
The Ohio State University

Honors and Awards

2017-18 Honors Research Scholarship, College of Engineering
The Ohio State University

2016-18 Kettering Scholarship, Department of Biomedical Engineering
The Ohio State University

2014-18 Eminence Fellows Scholarship
The Ohio State University

Fields of Study

Major Field: Biomedical Engineering

Table of Contents

Abstract iii
Dedication v
Acknowledgments vi
Vita vii
Table of Contents viii
List of Figures ix
Chapter 1. Introduction 1
1.1 Cancer Metastasis 1
1.2 DNA Origami 3
1.3 Microfluidics 4
1.4 Rationale 5
Chapter 2. Methods 7
2.1 DNA Origami Force Sensors 7
2.2 Microfluidic Devices 9
2.3 Experimental Technique 12
2.4 Imaging 13
Chapter 3. Results and Discussion 15
Chapter 4. Conclusions 22
4.1 Experimental Summary 22
4.2 Problems Encountered and Future Work 23
4.3 Contributions 26
Bibliography 27
Appendix A. DOFS Counting MATLAB Code 29
Appendix B. Supplemental AFM Images 31
Appendix C. Solution Preparation 32

List of Figures

Figure 1: Cancer cell migration phenotypes. 2
Figure 2: Double helical structure of DNA. 3
Figure 3: DOFS design process. 8
Figure 4: NanoDyn structure showing barrels and FRET linker. 8
Figure 5: Jablonski diagram showing donor and acceptor energy transfer. 9
Figure 6: Photolithography mask. 10
Figure 7: Soft lithography of PDMS. 11
Figure 8: Microfluidic device schematic. 12
Figure 9: Streptavidin on glass. Scale bar 10 μm. 15
Figure 10: Effect of streptavidin on DOFS binding. 16
Figure 11: DOFS counts at three different concentrations. 17
Figure 12: Example FRET image. Scale bar 10 μm. 18
Figure 13: DOFS in individual microchannel. 19
Figure 14: FRET pair activity. 19
Figure 15: Unbound and bound DOFS dwell times. 20
Figure 16: AFM image. One DOFS shown in red box. 21
Figure 17: FRET image showing DOFS aggregation in microfluidic device. 24
Figure 18: DOFS uptake by non-fluorescent MDA-MB-231 cells. 25
Figure 19: Zoomed in view of DOFS shown in Figure 16. 31
Figure 20: DOFS aggregation forming chains. 31

Chapter 1. Introduction

1.1 Cancer Metastasis

Metastasis, or the spread of malignant cancer cells from a primary tumor to secondary sites in the body, is responsible for up to ninety percent of cancer-related deaths.[1] As such, the mechanisms behind metastasis are of significant research interest. Cancer metastasis begins when cells in a tumor acquire an aggressive phenotype upon receiving cues from the microenvironment. These cells may breach the basement membrane of the epithelium and begin migrating through the tumor ECM to reach the circulatory system, at which point they intravasate and gain access to nearly any organ in the body.[2] The cells flow through the circulation and may become lodged in capillaries in distant organs, and can extravasate to form secondary tumors.[2]

For cells to migrate and begin intravasation, they can degrade the ECM to create channels, or may navigate through tracks made by other cells. Multiple single-cell migration phenotypes have been observed at this stage, including mesenchymal and amoeboid migration. These contrasting phenotypes are shown below in Figure 1. Mesenchymal migration, shown in panel (a), is a well-understood process involving pseudopod protrusion, the formation of focal contacts, proteolysis of the ECM, actomyosin contraction, and detachment of the trailing edge.[2] Amoeboid migration, shown in panel

(b), differs in that amoeboid migration involves subcellular blebbing primarily due to actomyosin contraction.[2]

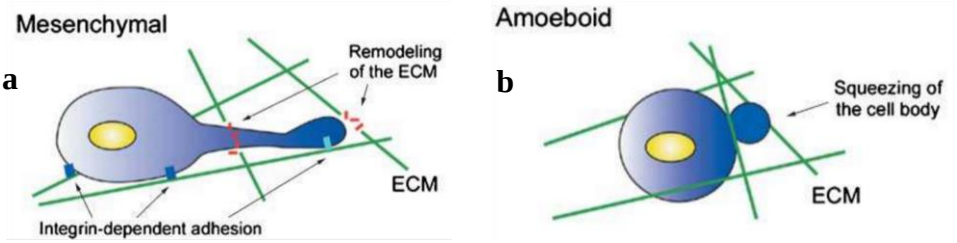

Figure 1: Cancer cell migration phenotypes.

High cell confinement and low focal adhesions have been shown to favor the amoeboid mechanism. This limits the ability of cells to spread out and adhere to the substrate, which increases migration speed by narrowing and aligning traction forces. Anti-cancer drugs that inhibit protease function have been shown to drive invasive cells toward another phenotype called amoeboid migration, where cells navigate via subcellular blebbing and can travel up to 30 times faster than possible in mesenchymal modalities by creating fewer focal contacts on the substrate.[3] As such, the stereotypic convergence toward amoeboid migration shows this modality may serve as a drug-resistance mechanism.[2,3]

Cells undergoing amoeboid migration are known to exert significant push forces normal to the substrate.[4] Advances such as Cellular Traction Force Microscopy (CTFM), where cells displace fluorescent beads on *in vitro* planar substrates, have been useful in studying cell force mechanics. However, this approach is largely limited to 2 dimensions, and the measured forces are often in directions parallel to the substrate.[5,6] As a result, there is a gap in our understanding of amoeboid migration mechanisms.

1.2 DNA Origami

Deoxyribonucleic acid, or DNA, is the genetic material of our cells. The information stored within DNA is responsible for coding for proteins that have innumerable functions in the body. DNA is well-known for its double-helical shape, first discovered by Watson and Crick in 1953 and further elucidated by Rosalind Franklin.[7] This double helix consists of adenine-thymine and guanine-cytosine base pairs and a sugar-phosphate backbone with a structure similar to that shown in Figure 2 below. The figure is of B-form DNA, the most common structure for DNA featuring major and minor grooves and a perpendicular orientation of the base-pairs. B-form DNA has a base-pair approximately every 0.34 nm, and makes one full 360° twist every 3.4 nm.

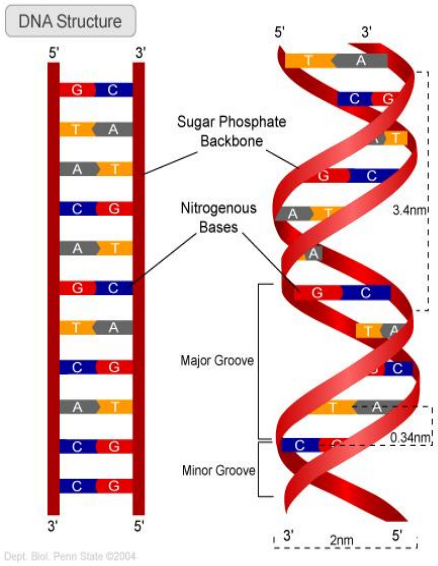

Figure 2: Double helical structure of DNA.

Pioneered by Nadrian Seeman in the early 1980's, DNA nanotechnology began with manipulating selective Watson and Crick base pairing to create immobile DNA junctions.[8] Rothemund in 2006 showed it was possible to use a single-stranded DNA scaffold to develop self-assembling DNA origami structures 100 nm in diameter.[9] Dietz

and coworkers advanced this work and introduced base pair additions and deletions into DNA origami to introduce stresses that bent the structures.[10]

Using these techniques, our associates at the Nanoengineering and Biodesign Laboratory, led by Dr. Carlos Castro, have exploited the mechanical stress in DNA nanostructure design and developed a DNA origami force sensor (DOFS) capable of measuring forces at 10 pN resolution. The sensor contains two fluorescent dyes, one red that excites when the two DNA barrels of the structure are pushed close together, and one green that excites when the barrels are far apart. Without applied force, the sensor is free to transition between the open and closed states, but the open state predominates. When a force is applied to the end of the sensor, the barrels cannot move away from the closed state and red fluorescence is observed. Tracking the open and closed states of the DOFS allows nanoscale force measurement. Further description of the NanoDyn DOFS structure is provided by Hudoba et al.[11–13]

1.3 Microfluidics

Microfluidics is a form of lab-on-a-chip technology where systems containing microscale channels are used to manipulate microliters to picoliters of fluids. The field first developed out of techniques used in molecular analysis and molecular biology.[14] Together, these fields share the goal of obtaining useful information with limited quantities of sample. The microelectronics industry, through the technique of photolithography, or the manufacturing of semiconductors using silicon wafers, provided a way to make microfluidic systems efficiently.[14] However, since the materials for microelectronics are not biocompatible, most work has focused on using polydimethylsiloxane, or PDMS, a soft

elastomer that is permeable to gases. Thus, PDMS is better able to support cells for *in vitro* experiments.

In recent years, microfluidics has evolved to a major research discipline, with applications in studying blood flow, cancer cell migration, and angiogenesis, among others.[14–16] Microfluidic systems are often used because they allow for high-throughput *in vitro* studies that are less expensive and more controllable than other 2D and 3D platforms.[16]

1.4 Rationale

By combining the techniques of microfluidics and DNA origami, we have conducted a proof-of-concept study and developed a method to measure cellular traction forces in 3 dimensions. As mentioned previously, there is a gap in our understanding of amoeboid migration mechanisms on a subcellular scale due to limitations with CTFM and other methods of studying mechanotransduction.

A study by Legant et al. showed that it was possible to embed cells in a 3D PEG hydrogel and tracked the displacement of fluorescent beads to calculate traction forces.[17] Another study by Gjorevski et al. embedded cells in a 3D type I collagen network and mapped traction forces throughout the surrounding hydrogel matrix.[18] However, Zhang et al. comment that these studies are limited in that some cancer cells and fibroblasts may degrade and remodel this ECM during migration, changing the properties of the ECM and making accurate traction force measurement difficult.[19]

The present study aims to address some of these challenges. Techniques based on fluorescence resonance energy transfer (FRET) to detect subcellular mechanotransduction

have been shown to allow for high sensitivity and force measurement on a picoNewton scale. By incorporating FRET into a DNA origami force sensor and coating microfluidic devices with these structures, we aimed to generate 3D “heat-maps” of cell migration in real time.

Chapter 2. Methods

2.1 DNA Origami Force Sensors

DNA origami force sensors (DOFS) are fabricated using techniques developed by our collaborators in the Nanoengineering and Biodesign Laboratory. The design of the NanoDyn was performed by Michael Hudoba using the caDNAno software program. The first component of the DOFS is the scaffold that serves as the backbone of the structure, often shown as cylinders (Figure 3A).[13] Here we use M13mp18 that is 7249 bases in length. The scaffold winds through the entire DNA structure but is designed to not bind to itself (Figure 3B).[13] Instead, the scaffold binds to a large number of staple strands, each about 30-50 bases in length, that bind to separate regions on the scaffold (Figure 3C).[13] The staples are designed to be complimentary to the scaffold strand, thus causing the DNA to become double-stranded after binding (Figure 3D). About 175 unique staples are used in the NanoDyn structure.

The DNA staples are custom-ordered in stock plates, and are then combined in specific ratios into a working stock. The folding is set up to make a final concentration of 20 μM scaffold in a buffer of 1 mM EDTA, 5 mM NaCl, 5 mM Tris, and 11 mM $MgCl_2$. The solution is then thermally annealed starting at 65°C and cooled to 4°C over three days. Upon thermal annealing, the short staples bind to the scaffold, and pull the scaffold into a 3-dimensional shape shown below in Figure 4.

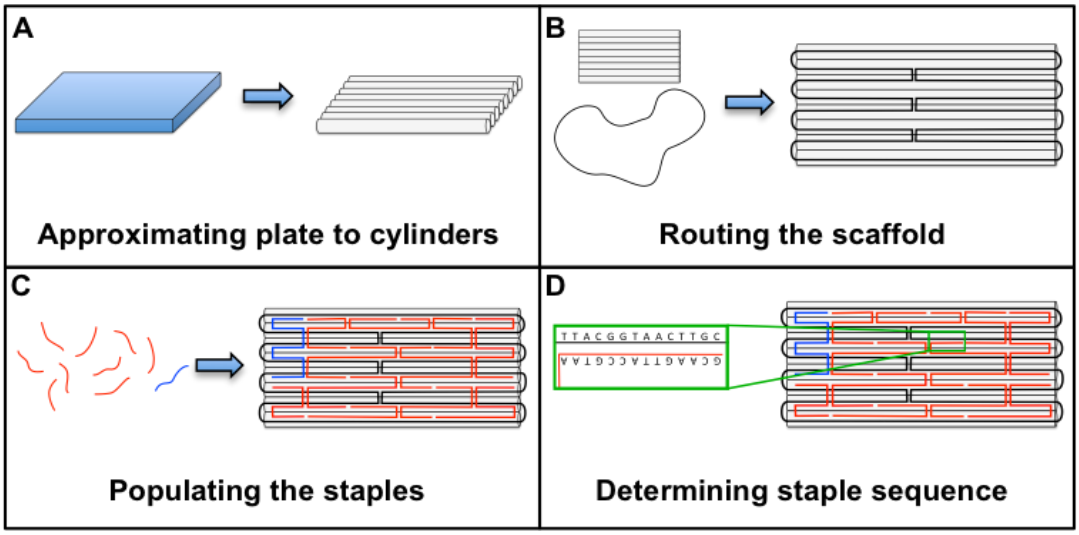

Figure 3: DOFS design process.

Of note in the structure below is the presence of single stranded linkers between the top and bottom barrels of the structure. This linker contains two fluorescent dyes that are able to undergo Förster Resonance Energy Transfer (FRET). As shown in the Jablonski diagram in Figure 5, the donor fluorophore, after excitation to the S_1 state, can either emit fluorescence and return to the S_0 state, or if the acceptor is nearby, transfer its energy to the

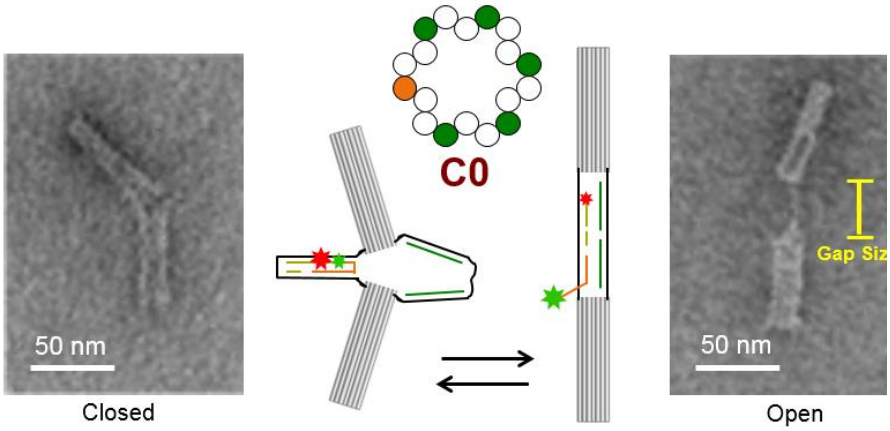

Figure 4: NanoDyn structure showing barrels and FRET linker.

acceptor.[20] The acceptor fluorophore is raised to the S_1 state, and will then emit a different fluorescent color and return to the S_0 state.[20]

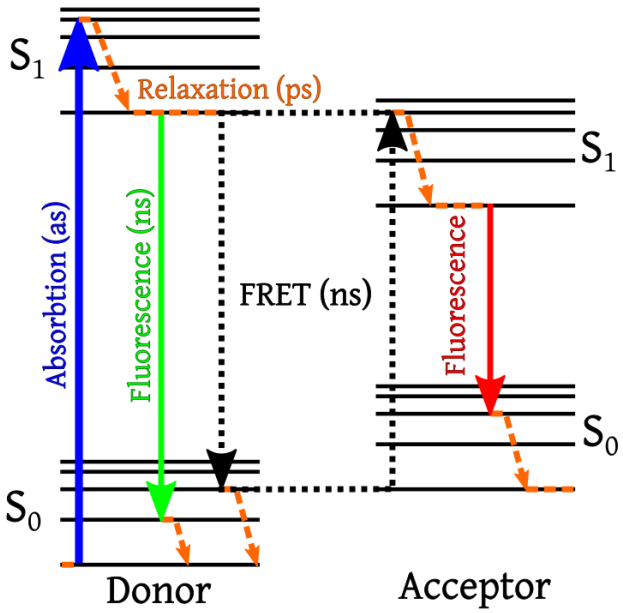

Figure 5: Jablonski diagram showing donor and acceptor energy transfer.

In the NanoDyn, Cy3 is used as the FRET donor, and Cy5 is used as the FRET acceptor. The NanoDyn is designed to bend at the single-stranded linker region at an applied compressive force of about 10 pN, as seen in Figure 4. This change in conformation causes the donor and acceptor to be pushed near each other. As a result, when the donor is excited by a 561 nm laser during DOFS compression, FRET occurs and Cy5 emission is observed around 640 nm.

2.2 Microfluidic Devices

Development of the microfluidic devices used in these experiments begins with the drafting of a sketch in SolidWorks. The sketch is then converted to an AutoCAD drawing and sent to a company that produces a thin plastic mask. The mask is clear wherever the

features of the device are, and is black everywhere else. An example mask is shown below in Figure 6.

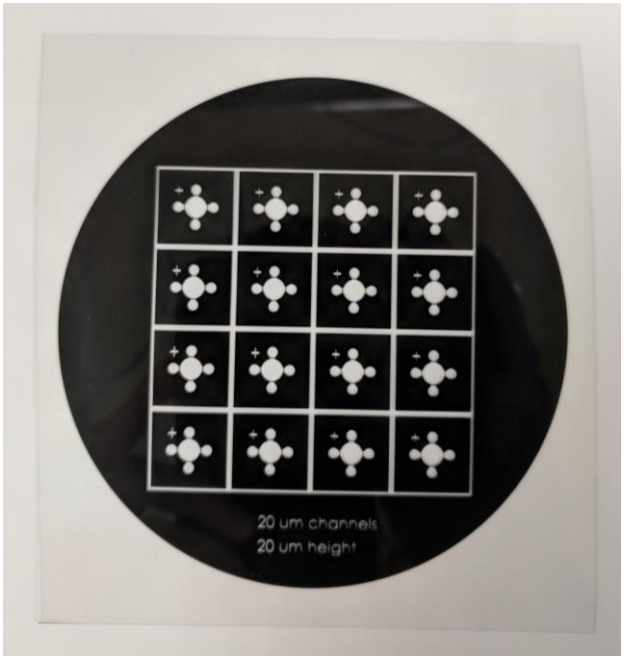

Figure 6: Photolithography mask.

Silicon wafers are purchased and developed in a cleanroom. The wafer is first spin-coated with a thin film of SU-8, an epoxy-based negative photoresist. The wafer is heated briefly before being placed under the plastic mask described previously. The mask and SU-8 coated wafer are then exposed to ultraviolet light. The ultraviolet light causes the epoxy molecules to crosslink, stiffening the polymer wherever the mask is clear. The wafers are removed from the aligning machine, and excess SU-8 is washed off using isopropyl alcohol. After a final heating, wafers are exposed to silane using a vacuum chamber in our laboratory. The silane coating prevents the following soft lithography steps from removing the SU-8 features on the surface.

PDMS is mixed using a 10:1 ratio of solution to curing agent. The PDMS is placed in a vacuum to remove excess air bubbles before the solution is poured onto a silicon wafer. Excess air bubbles are again removed using a vacuum before the wafer is placed in a 65°C oven overnight. The features on the silicon master create indented channels in the cured PDMS. This process is shown below in Figure 7.[21]

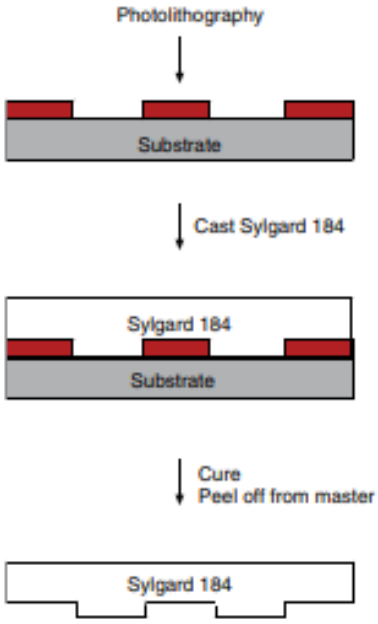

Figure 7: Soft lithography of PDMS.

PDMS devices are cut from the master using a scalpel, and holes are punched in the devices using 1.5 mm and 4 mm biopsy punches. These holes made in the PDMS enable access for culture media and cells to be added to the microchannels for our experiments. The devices are cleaned with packaging tape to remove dust and debris, and are then placed in a plasma chamber along with thin, clean glass slides. A vacuum pump is used to lower the pressure in the chamber to 600 millitorr before the plasma coil is activated. Exposure to plasma for one minute and thirty seconds causes the surfaces of the

glass and PDMS to become hydrophilic. After the devices are removed, the exposed surfaces are bonded together to create enclosed chambers.

A diagram of the microfluidic device used in our work is shown in Figure 8. Between the center and edge ports seen on the device as circles there are rows of microchannels each 20 µm wide by 250 µm long.

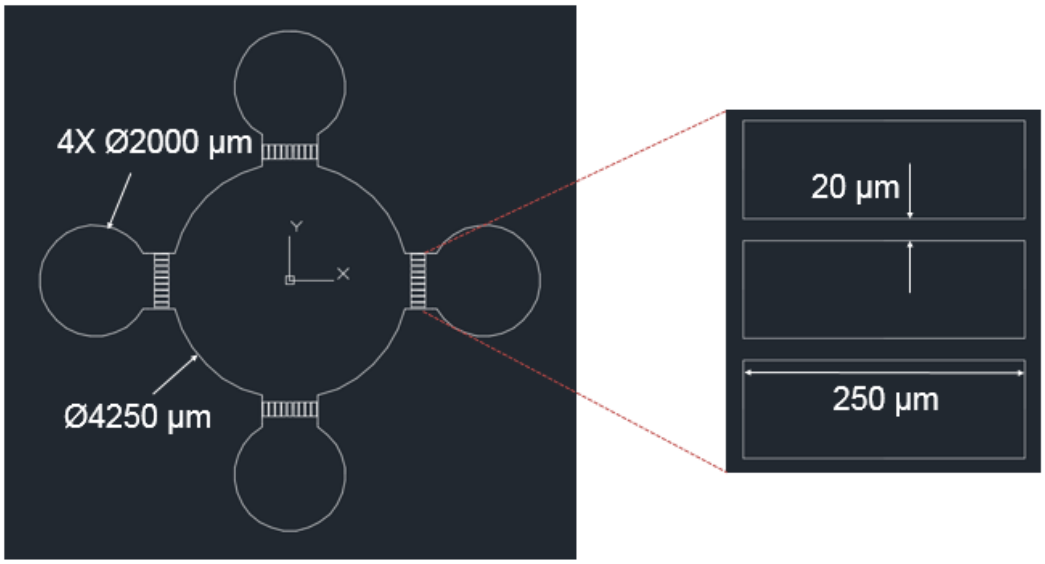

Figure 8: Microfluidic device schematic.

2.3 Experimental Technique

To prepare the devices for experiments, 20 µL of 100 µg/mL streptavidin is flushed into the middle circular port immediately after bonding. After five minutes, the device is flushed with phosphate-buffered saline, or PBS, and aspirated in all ports with a pipette and vacuum pump. 20 µL of 10 µg/mL casein is then added to the device in the center port, and after five minutes, the device is flushed with PBS once again. After aspiration, 20 µL of DOFS structures diluted to 1 nM with FOB are injected into the middle port of the device.

Streptavidin is a protein with a high affinity for biotin.[22] The DOFS are functionalized with biotin at the end of each barrel after fabrication. Thus, when the DOFS are flushed into the center port, the pressure gradient between the full center port and empty edge ports forces the structures through the device. Streptavidin has four binding sites for biotin; thus, when the DOFS are added, they irreversibly bind with the streptavidin.[22] This creates 3-dimensional channels lined with sensors that change their fluorescence when forces are exerted on them by migrating or adhering cells.

The cells used in these experiments are MDA-MB-231 breast cancer cells cultured in DMEM with 4.5 g/L D-Glucose and L-Glutamine, and 110 mg/L Sodium Pyruvate supplemented with 10% FBS and 1% Penicillin/Streptomycin. MCF10A human mammary epithelial cells are used as controls. Other trials have used MIA-PaCa-2 pancreatic cancer cells, and SCP2 modified breast cancer cells cultured in appropriate media.

2.4 Imaging

Devices are imaged using a total internal reflection microscope (TIRF). The glass slide and microfluidic device are placed on the stage of the microscope. The microscope is set to shine a laser at approximately a 20° angle through the sample. The light is internally reflected through the sample, creating a focal plane of about 100 nm, before the light returns to the detector. The microscope is also capable of performing FRET using a beam splitter and dichroic mirror.

AFM imaging is carried out in collaboration with the Micro/Nano Multiphysical Dynamics Lab led by Dr. Hanna Cho. Thin glass slides are plasma oxidized before streptavidin and casein are applied similar to the techniques described previously. The

DOFS are deposited onto glass slides and allowed to adhere for 1 hour before washing with FOB. Images were captured using an Asylum Research MFP-3D-Infinity.

Chapter 3. Results and Discussion

Initial work focused on optimizing the binding of streptavidin in the microfluidic channels. Serial dilutions of streptavidin were done, ranging from 200 µg/mL to 20 ng/mL. High concentrations of streptavidin, above 20 µg/mL, resulted in coverage such as that shown below in Figure 9. Here, most of the glass substrate is covered in streptavidin with little extra space.

While many trials were conducted to determine which concentrations of streptavidin would be best suited to allow for a 1:1 strep to DOFS binding ratio, later work showed that excess streptavidin, around 200 µg/mL, provided better surface coverage, and allowed for DOFS to bind in greater amounts.

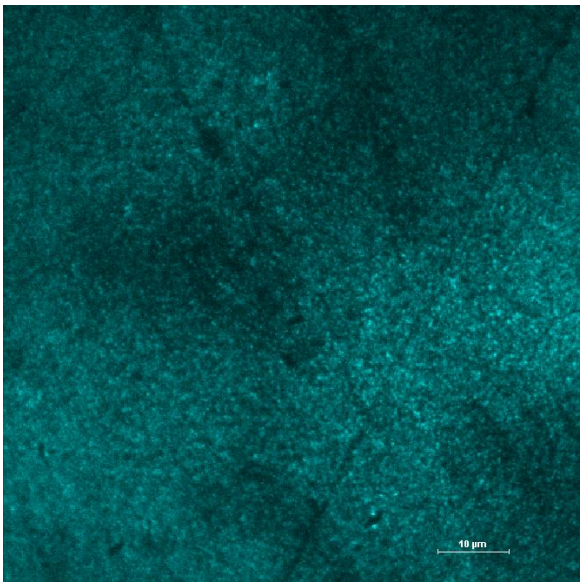

Figure 9: Streptavidin on glass. Scale bar 10 µm.

Experiments were also conducted to determine whether streptavidin had a statistically significant effect on DOFS binding. Since DOFS can theoretically bind to glass without any other adhesion molecules, the experiments were conducted to see if DOFS binding was greatly assisted through a streptavidin intermediate. Three devices each were fabricated for streptavidin only and streptavidin with DOFS. After washing with FOB, the devices were imaged with the TIRF microscope, and five images were captured for each device. Custom MATLAB software, shown in Appendix A, was used to automatically count how many sensors were present using grey level thresholding. As shown below in Figure 10, the DOFS only condition had a median binding of about 4

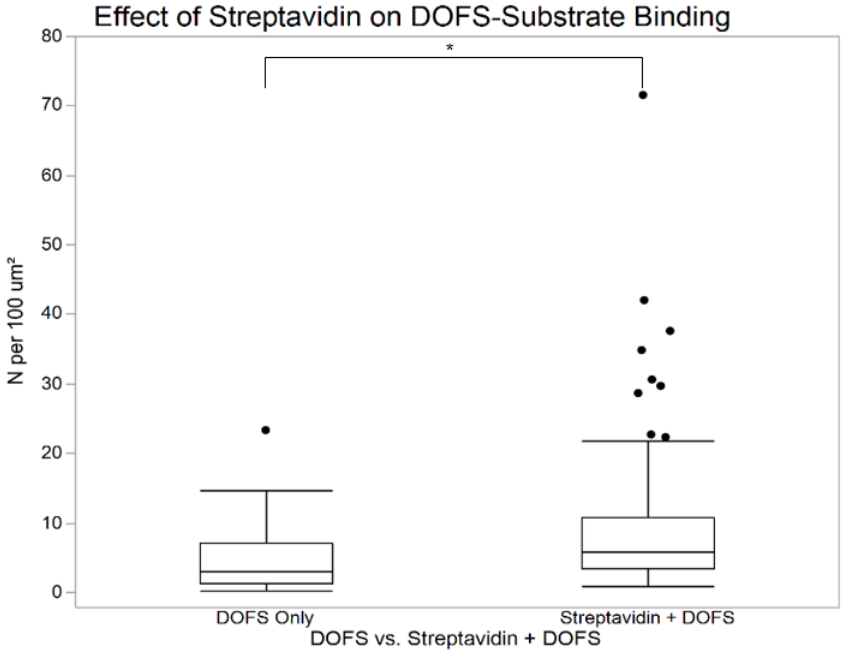

Figure 10: Effect of streptavidin on DOFS binding.

sensors per 100 μm^2, while the streptavidin increased this by two fold to about 8 sensors per 100 μm^2. This was determined to be statistically significant using a Wilcoxson rank

test for difference in medians. This supported the use of streptavidin in further experiments to increase DOFS binding.

The DOFS attachment was also optimized independently. Three devices were fabricated each for 1 nM (1000 pM), 100 pM, and 10 pM DOFS. Ten images were captured for each concentration, and the same MATLAB code used previously was used to count DOFS attachment. As seen in the graph below, 1 nM DOFS had the highest concentration of about 32 sensors per 100 μm^2. Higher concentrations were not tested due to limitations during structure preparation. In addition, higher concentrations resulted in DOFS crowding that made it difficult to distinguish between individual structures. Therefore, 1 nM DOFS were used in subsequent experiments.

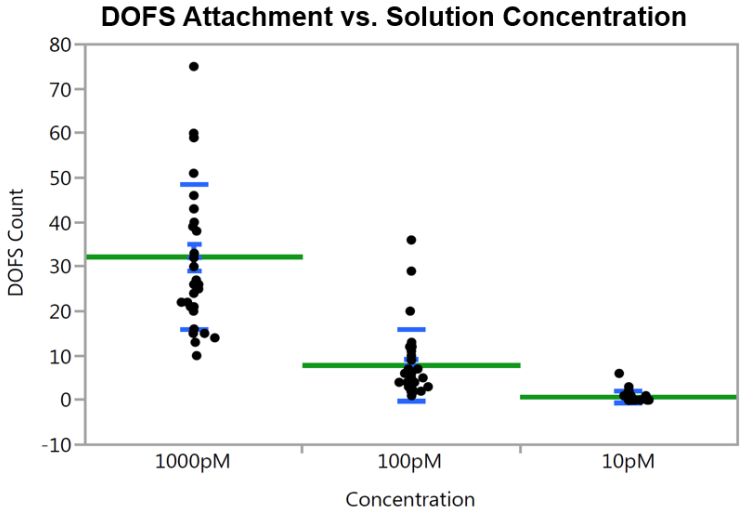

Figure 11: DOFS counts at three different concentrations.

FRET images were acquired using the TIRF microscope and attached FRET camera as detailed previously. An example FRET image is shown in Figure 12 below. The left panel shows the open state of the force sensor, expressing fluorescence at a 561 nm

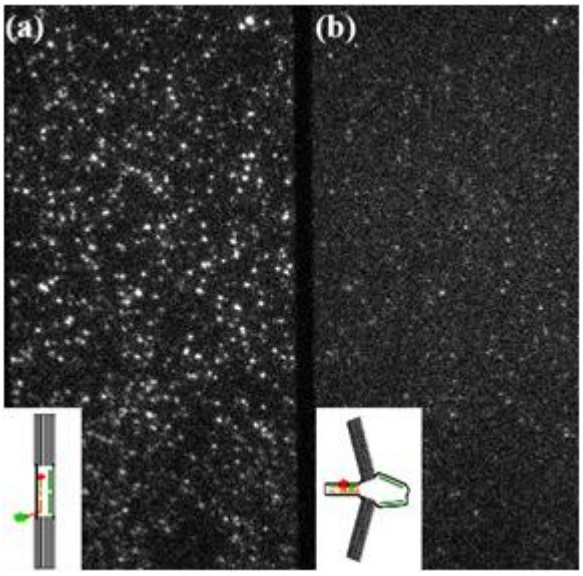

Figure 12: Example FRET image. Scale bar 10 μm.

excitation, while the right panel shows the closed state of the sensor with fluorescence at a 640 nm excitation. Ideally, the sensor with no constraining linkers should be in the open state when no forces are applied, and in the closed state when tensional forces are applied.

Figure 13 below shows DOFS in an individual microchannel. From the image, it can be seen that DOFS tended to distribute fairly evenly, with moderate adherence to channel walls. In line with expected behavior, most DOFS remained in the open state, seen in the left panel, since no cells were present.

Additional MATLAB code was used to track the DOFS through timelapse imaging. In brief, the code used background subtraction followed by alignment of the donor and acceptor channels to match the pairs through a timelapse. The outputs of the code were graphs of each FRET pair activity over time and a graph of dwell times, or how long the sensor stayed in the open and closed configurations. Example images of individual FRET

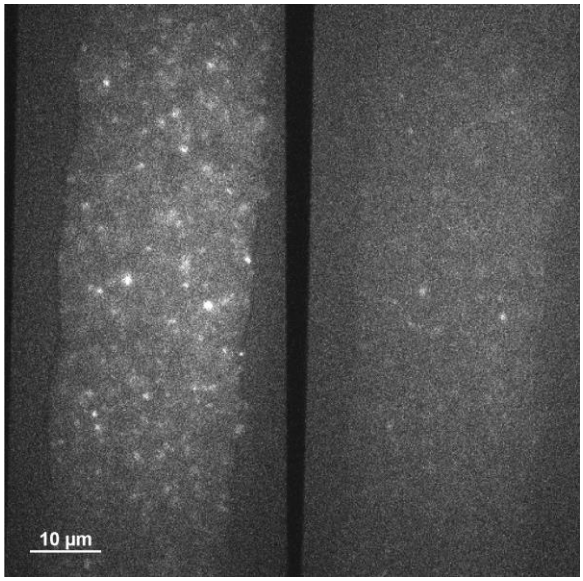

Figure 13: DOFS in individual microchannel.

pair activity and dwell times are shown in Figure 14 and Figure 15 below. In Figure 14 the top panel is raw pixel brightness and the bottom panel is normalized intensity.

It can be seen from the Figure 14 that this pair spent most of its time in the open state with donor excitation. Around frame 300, the donor photobleached and no more signal is obtained. Example graphs of dwell times for the Nanodyn as obtained by Dr. Hudoba are shown in Figure 15.[11] The pink graph represents the open state of the DOFS,

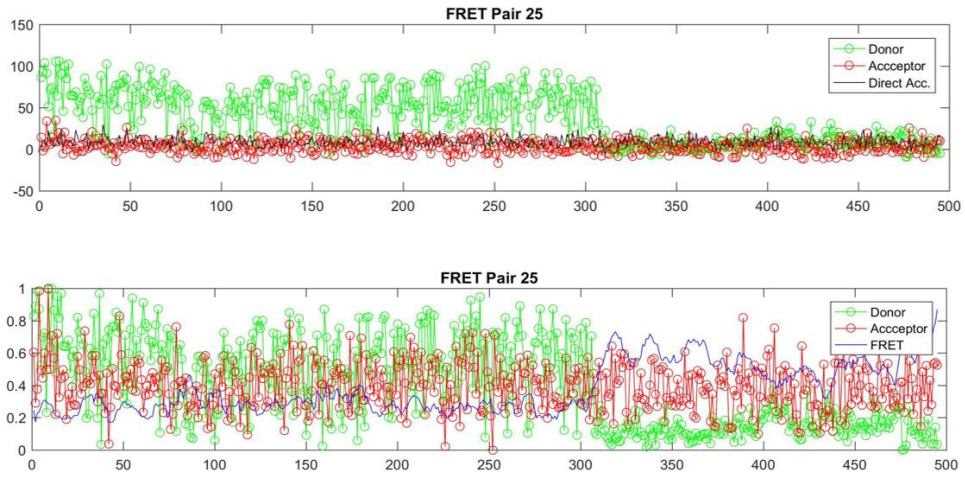

Figure 14: FRET pair activity.

while the blue graph represents the closed state. As seen in the graphs, the force sensor tended to spend more time in the open state than closed state. Similar graphs would be expected to be obtained in our DOFS experiments based on our obtained microchannel images.

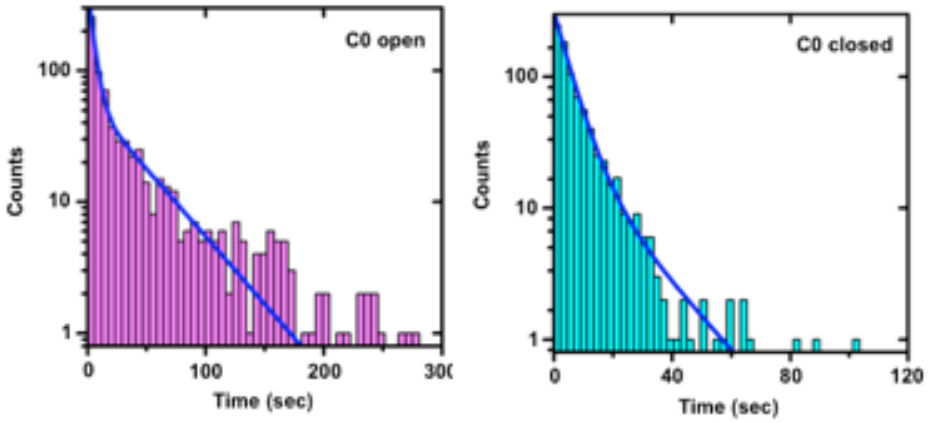

Figure 15: Unbound and bound DOFS dwell times.[11]

DOFS were also imaged using atomic force microscopy in tapping mode. Devices were imaged on glass with no buffer present. An example AFM image is shown in Figure 16 below. As seen in the image, the DOFS tended to be horizontal on the substrate. This indicates that the DOFS would be capable of measuring cell-generated shear forces rather than normal forces. Other AFM images showed DOFS tended to cluster and form aggregates. The DOFS tended to aggregate with the end of one device touching the end of another device, forming strips of DOFS that bent and connected with other strips. An example image is provided in Figure 20 in Appendix B. Future work must be done to explore this further. Additional AFM images are provided in Appendix B, including a zoomed in view of the DOFS in Figure 16.

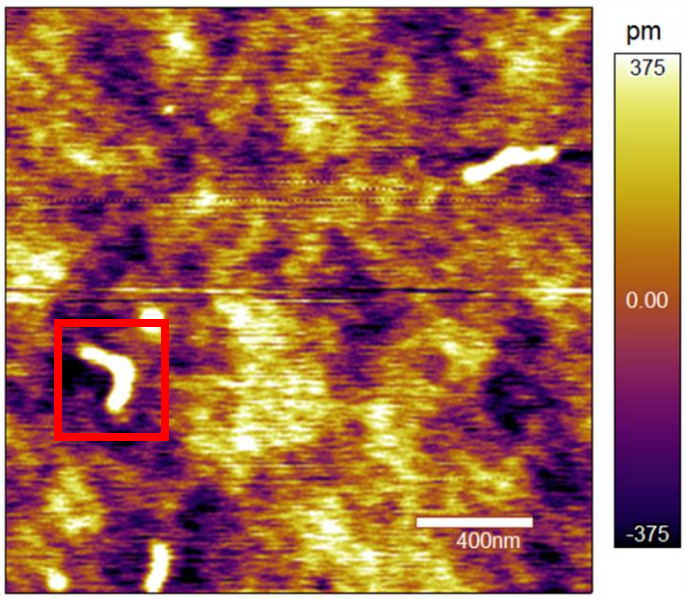

Figure 16: AFM image. One DOFS shown in red box.

Chapter 4. Conclusions

4.1 Experimental Summary

The purpose of this work was to develop and test a system for measuring cell generated forces in 3-dimensional microchannels to gain a better understanding of amoeboid migration mechanisms *in vivo*. The effect of streptavidin was first analyzed, followed by the concentration of the DOFS. DOFS binding with streptavidin had a significantly higher concentration than DOFS on glass alone, with a p-value less than 0.05. Further, DOFS concentrations around 1 nM were beneficial for ensuring high coverage, while higher concentrations and some tests with 1 nM caused DOFS aggregation. The devices were imaged using TIRF microscopy to study dwell times of the sensors in the open and closed states, and the devices were analyzed with an AFM to determine that they are best suited for measuring shear forces.

This system provides a platform for studying cancer cell migration forces in a microfluidic system. Microfluidic systems are cheap to fabricate and allow for greater geometric and chemical control than other *in vitro* systems. Streptavidin and DOFS can be added to microfluidic devices efficiently and effectively, and they are capable of binding in 3-dimensions in confined channels.

Recent studies have shown migrating cancer cells undergo a transition to amoeboid migration when confined in channels less than 10μm in width.[23,24] This platform could be used in microfluidic channels 10 μm in height and having widths of 5 μm, 10 μm, 20 μm,

and 50 μm that mimic mechanical confinement. Fluorescent readouts of the DOFS may be compared to real-time or timelapse movies of cell migration to produce dynamic force maps of metastatic and normal cell migration as a function of microchannel confinement. This work has applications in addressing the limitations of conventional 2D and some 3D CTFM. By harnessing the ability of DOFS to bind in 3 dimensions in confined microchannels, cells could be tracked and results could be analyzed to determine the effects of the amoeboid migration phenotype on cellular traction forces.

4.2 Problems Encountered and Future Work

The effects of streptavidin on DOFS binding were explored early in this research. Streptavidin is a tetramer, and thus is known to have four binding sites for biotin.[22] Therefore, it was expected that at least one DOFS would bind per avidin molecule. However, streptavidin aggregation and uneven DOFS distribution led to the ratio of DOFS to streptavidin molecules to be much less than one. This did not end up affecting later work, since excess streptavidin should only be beneficial to increase DOFS binding.

The DOFS were found to aggregate when added to our microfluidic devices in high amounts. Images such as Figure 17 show how DOFS can completely coat the surface of microfluidic channels when added at concentrations near and above 1 nM. While aggregation could potentially be beneficial for increasing the number of DOFS per cell for measuring migration forces, high sensor counts make quantification difficult. Indeed, the MATLAB code used to count DOFS and measure FRET signals over time relies on identifying individual structures between both FRET panels. High DOFS counts prevent the code from obtaining accurate measurements as individual DOFS are impossible to

distinguish in large clusters. It is possible that concentrations of 300-500 pM DOFS may be more appropriate for ensuring adequate coverage while minimizing clustering.

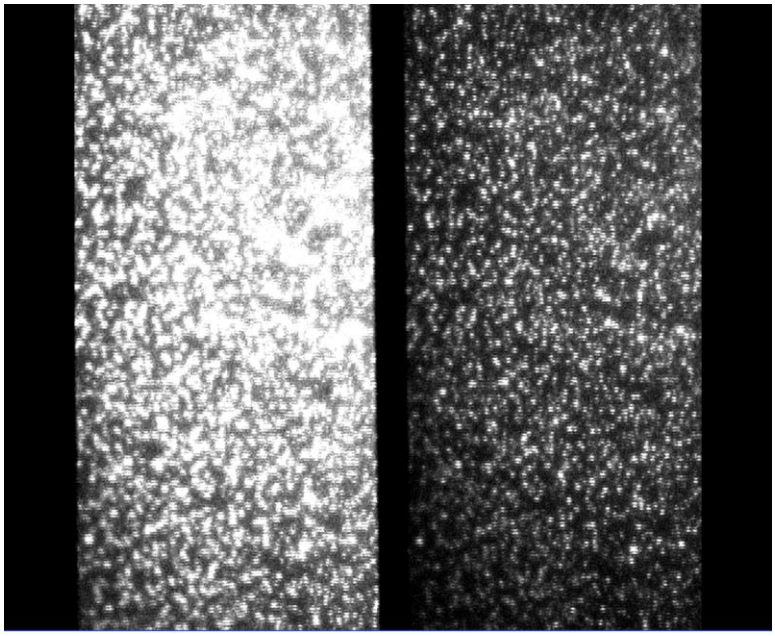

Figure 17: FRET image showing DOFS aggregation in microfluidic device.

Another issue was that cells imaged simultaneously with DOFS interfered with DOFS analysis. Indeed, some cells appeared to internalize the DNA structures, while others exhibited their own fluorescence in the 561 nm range that made tracking individual DOFS with our MATLAB code difficult. Even with fully non-fluorescent MDA-MD-231 cells, the high intensity laser from the TIRF microscope caused vesicles in the cells to appear to fluoresce brightly, as shown below in Figure 18. This could be alleviated through optimizing the FRET pair of the DOFS, as well as optimizing the focal plane for imaging to excite the DOFS without exciting the cells above.

Further, as noted from the AFM experiments, DOFS appeared to be oriented parallel to the glass substrate. Therefore, they would be able to measure shear forces rather

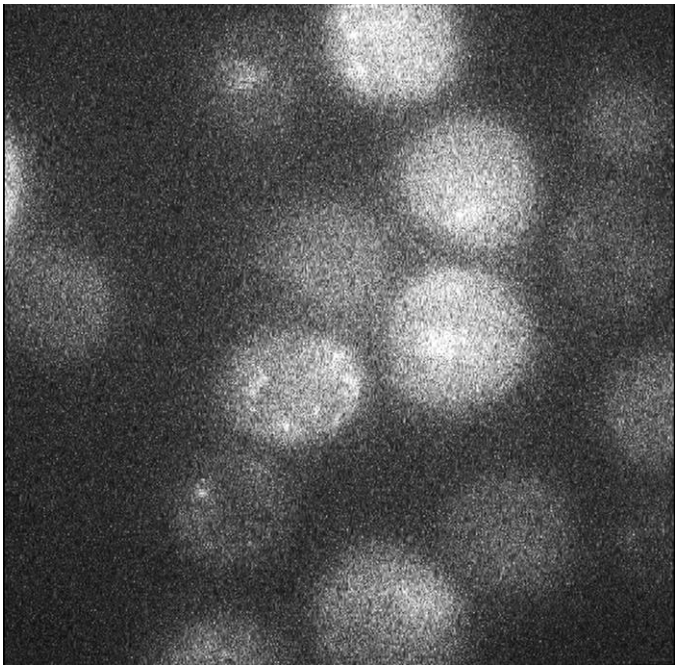

Figure 18: DOFS uptake by non-fluorescent MDA-MB-231 cells.

than normal forces. However, amoeboid and other modes of cell migration may include significant forces normal to the substrate as these cells remodel and move through the ECM. It is possible that contact mode or tapping mode with the AFM both result in DOFS being distorted to appear horizontal due to applied forces from the AFM tip. However, future work should include more AFM imaging, perhaps with the addition of tunneling electron microscopy, to determine whether DOFS are tangential or normal to the surface in migration studies. In addition, additional AFM images should be captured on mica using agarose gel-purified DOFS.

Lastly, to further elucidate the coverage of DOFS in 3 dimensions, microfluidic systems should be imaged using confocal microscopy. Z-stack images should be captured of the microfluidic device, including the glass substrate and 20 μm square channels. The DOFS appear to coat the walls based on acquired TIRF images, yet confocal imaging

would allow this to be verified and allow for further optimization of the DOFS coating protocol.

As an additional application of this research, the system we have developed could be used as a drug-screening platform. Cancer cells could be tracked using our 3D force mapping techniques with DOFS, and representative heat-maps as a function of mechanical confinement could be generated. Then, different drugs such as taxol that interfere with microtubule polymerization could be applied to these cancer cells, and the resulting response could be measured. For instance, cells may show reduced migration due to taxol, and the platform developed in this research would provide a way to obtain subcellular, quantitative information on how exactly the forces involved in cell migration change.

4.3 Contributions

DOFS were developed by Hudoba et al. in the Nanoengineering and Biodesign Laboratory led by Carlos Castro, PhD. I designed the microfluidic devices used in these experiments and developed the protocol for binding the DOFS with streptavidin in the microfluidic chambers. Guidance for this project was provided by Jonathan Song, PhD, Carlos Castro, PhD, Michael Hudoba, PhD, Ayush Garg, and Ehsan Akbari. AFM imaging was conducted with Jinha Kwon in the Micro/Nano Multiphysical Dynamics Lab led by Hanna Cho, PhD.

Bibliography

1. Gupta, G. P. & Massagué, J. Cancer Metastasis: Building a Framework. *Cell* **127,** 679–695 (2006).

2. Friedl, P. & Wolf, K. Tumour-cell invasion and migration: diversity and escape mechanisms. *Nat. Rev. Cancer* **3,** 362–374 (2003).

3. Wolf, K. *et al.* Compensation mechanism in tumor cell migration: mesenchymal–amoeboid transition after blocking of pericellular proteolysis. *J. Cell Biol.* **160,** 267–277 (2003).

4. Álvarez-González, B. *et al.* Three-Dimensional Balance of Cortical Tension and Axial Contractility Enables Fast Amoeboid Migration. *Biophys. J.* **108,** 821–832 (2015).

5. Munevar, S., Wang, Y. & Dembo, M. Traction force microscopy of migrating normal and H-ras transformed 3T3 fibroblasts. *Biophys. J.* **80,** 1744–1757 (2001).

6. Sabass, B., Gardel, M. L., Waterman, C. M. & Schwarz, U. S. High Resolution Traction Force Microscopy Based on Experimental and Computational Advances. *Biophys. J.* **94,** 207–220 (2008).

7. Watson, J. D. & Crick, F. H. Molecular structure of nucleic acids; a structure for deoxyribose nucleic acid. *Nature* **171,** 737–738 (1953).

8. Seeman, N. C. Nucleic acid junctions and lattices. *J. Theor. Biol.* **99,** 237–247 (1982).

9. Rothemund, P. W. K. Folding DNA to create nanoscale shapes and patterns. *Nature* **440,** 297–302 (2006).

10. Dietz, H., Douglas, S. M. & Shih, W. M. Folding DNA into Twisted and Curved Nanoscale Shapes. *Science* **325,** 725–730 (2009).

11. Hudoba, M. W. Force Sensing Applications of DNA Origami Nanodevices. (The Ohio State University, 2016).

12. Hudoba, M. W., Luo, Y., Patton, R., Poirier, M. G. & Castro, C. Entropically Controlled Nanomechanical DNA Origami Devices. *Biophys. J.* **110,** 656a (2016).

13. Hudoba, M. W., Luo, Y., Zacharias, A., Poirier, M. G. & Castro, C. E. Dynamic DNA Origami Device for Measuring Compressive Depletion Forces. *ACS Nano* **11,** 6566–6573 (2017).

14. Whitesides, G. M. The origins and the future of microfluidics. *Nature* **442,** 368–373 (2006).

15. Akbari, E., Spychalski, G. B. & Song, J. W. Microfluidic approaches to the study of angiogenesis and the microcirculation. *Microcirculation* **24,** e12363 (2017).

16. Sung, K. E. & Beebe, D. J. Microfluidic 3D models of cancer. *Adv. Drug Deliv. Rev.* **79–80,** 68–78 (2014).

17. Legant, W. R. *et al.* Measurement of mechanical tractions exerted by cells in three-dimensional matrices. *Nat. Methods* **7,** 969–971 (2010).

18. Gjorevski, N. & Nelson, C. M. Mapping of Mechanical Strains and Stresses around Quiescent Engineered Three-Dimensional Epithelial Tissues. *Biophys. J.* **103,** 152–162 (2012).

19. Zhang, Y. *et al.* Progress in Integrative Biomaterial Systems to Approach Three-Dimensional Cell Mechanotransduction. *Bioengineering* **4,** 72 (2017).

20. *Principles of Fluorescence Spectroscopy*. (Springer US, 2006). doi:10.1007/978-0-387-46312-4

21. Qin, D., Xia, Y. & Whitesides, G. M. Soft lithography for micro- and nanoscale patterning. *Nat. Protoc.* **5,** 491–502 (2010).

22. Weber, P. C., Ohlendorf, D. H., Wendoloski, J. J. & Salemme, F. R. Structural origins of high-affinity biotin binding to streptavidin. *Science* **243,** 85–88 (1989).

23. Liu, Y.-J. *et al.* Confinement and Low Adhesion Induce Fast Amoeboid Migration of Slow Mesenchymal Cells. *Cell* **160,** 659–672 (2015).

24. Lämmermann, T. & Sixt, M. Mechanical modes of 'amoeboid' cell migration. *Curr. Opin. Cell Biol.* **21,** 636–644 (2009).

Appendix A. DOFS Counting MATLAB Code

```
%*****************************************************
%* DOFS_Counting.m                                   *
%* Jacob Enders, Ayush Garg                          *
%* Microsystems for Mechanobiology and Medicine Lab *
%*****************************************************

%% Load Image, Split Channels
img = imread('testimage.png'); % Read image
figure(1), imshow(img) % Show original

%% Selecting Custom ROI in an Image
roi = imrect();
pos = wait(roi);
% pos = [64 64 384 384];
cropImg = imcrop(img, pos);
%cropImg = img;
%figure, imshow(cropImg), title('User Defined ROI')

% Background Subtraction
background = imopen(cropImg, strel('disk', 100));
i3 = rgb2gray(cropImg-background);

% Contrast Enhancement
i4 = i3;
%i4 = imadjust(i3);
figure(2), imshow(i4)

%% Background Filtering and Region Labeling
%level = graythresh(i4) (can use auto thresholding)
level = 0.4;
Ibw = im2bw(i4,level);

%Additional processing
Ibw = imfill(Ibw,'holes');
figure(3), imshow(Ibw), hold on
Ibw = bwareaopen(Ibw,4);
figure(4), imshow(Ibw), hold on
Ibw = bwmorph(Ibw,'spur');
figure(5), imshow(Ibw), hold on
label = logical(Ibw);

stat = regionprops(label, 'centroid','area')
N_initial = length(stat)

%% Calculations in pixels
% Do this in pixels
```

```
[m,n] = size(i4) % Find the dimensions of the selected area

area_list_pixels = cell2mat({stat(:).Area}'); % Isolate Area list from
stat struct

pixels_per_dofs = 3; % CHANGE THIS TO MODIFY SIZE OF 1 DOFS

% Divide all clusters by 4 pixels squared to get number of dofs in each
cluster
% Take the floor of each point to get a conservative estimate
% Add up to get total dofs count in area
N_countfinal_pixels = sum(floor(area_list_pixels/pixels_per_dofs))

% Divide number of clusters by area of image in pixels to get DOFS per
pixel squared
N_perpixel2 = N_countfinal_pixels/(m*n)

%% Calculations in microns
% Do this in microns
m_um = (10/57)*m; % 57 pixels per 10 microns means .17544 um per pixel
n_um = (10/57)*n;

area_list_um = cell2mat({stat(:).Area}'); % Isolate Area list from stat
struct
area_list_um = area_list_um.*((10/57)^2);

um_per_dofs = pixels_per_dofs*((10/57)^2);

% Divide all clusters by 4 pixels squared to get number of dofs in each
cluster
% Take the floor of each point to get a conservative estimate
% Add up to get total dofs count in area
N_countfinal_um = sum(area_list_um/um_per_dofs)

% Divide number of clusters by area of image in pixels to get DOFS per
pixel squared
N_perum2 = N_countfinal_um/(m_um*n_um)
N_perum100um2 = floor(N_perum2*100) % Number of sensors per 100 um
squared
```

Appendix B. Supplemental AFM Images

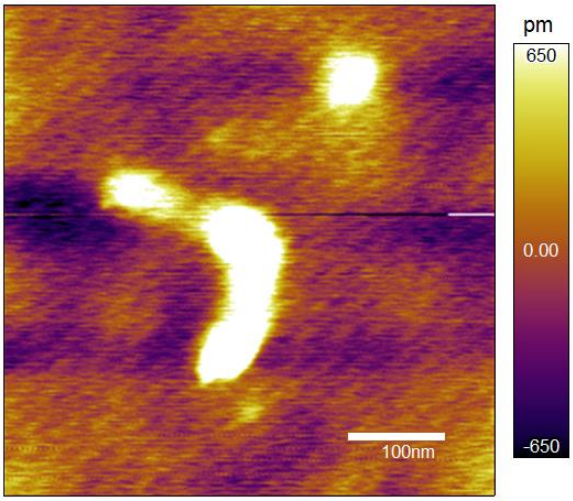

Figure 19: Zoomed in view of DOFS shown in Figure 16.

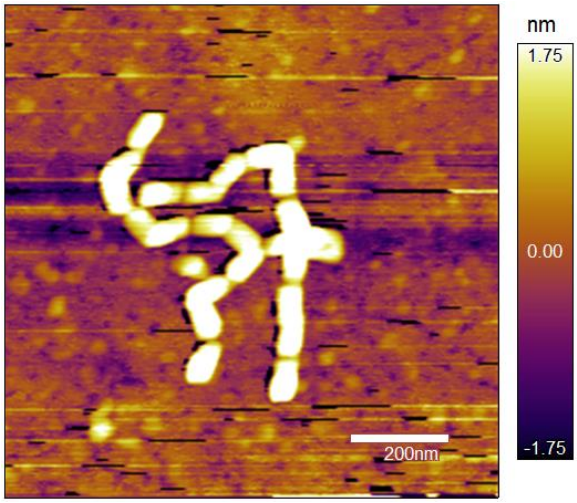

Figure 20: DOFS aggregation forming chains.

Appendix C. Solution Preparation

Preparation of Streptavidin:

1. Strep 488, volume is 10 uL, concentration 2 mg/mL
2. Serial dilutions, add 190 uL sterile PBS and mix thoroughly to get 100 uL at 0.1 mg/mL. Can store this for later use.
3. Take 10 uL of the 0.1 mg/mL solution and add to 0.2mL Eppendorf tube, add 90 uL PBS to get 100 ug/mL

Preparation of PEG 8000, 500 mM NaCl

1. Obtain 15 g of PEG, add 100 mL double distilled H_2O
2. Add 12.5 mL of 4 M NaCl solution
3. Mix thoroughly.

Preparation of 1x FOB, 11 mM $MgCl_2$

1. Obtain 5 mL of 10x FOB stock solution
2. Dilute with 45 mL of double distilled H_2O, total volume is 50 mL
3. Add 400 uL of 1.375 M $MgCl_2$ stock solution

Preparation of DOFS:

1. DOFS tube is 50 uL, add 50 uL PEG 8000, 500 mM NaCl and mix well
2. Take 100 uL mixture and transfer to 1.5 mL Eppendorf tube
3. Centrifuge at 16000 g, (16000 rcf) for 25 minutes, keeping track of the side of the tube facing up
4. Remove from centrifuge and carefully remove all liquid, keeping the DOFS area away from the pipet tip.
5. Add 50 uL of 1x FOB, 11 mM $MgCl_2$ to get 10 nM concentration of DOFS
6. Add 450 uL more FOB to get 1 nM concentration, standard working concentration
7. Add 5 uL of 0.1% v/v Tween-20 detergent to 500 uL DOFS and mix thoroughly